responses. To develop dynamic surfaces, PRX segments are necessary to be combined with hydrophobic anchoring terminal segments at both ends. Here, a random copolymer segment composed of MPC and BMA (PMB) was selected as an anchoring terminal (Fig. 1). The PMB segment is a well-known coating unit that can be stably immobilized on a hydrophobic material's surface to prevent non-specific biological responses.[27] To synthesize the PRX block copolymer, RAFT chain transfer agent (CTA) was initially introduced to PEG-bisamine, and pseudo-PRX macro CTA was synthesized with α-CD. Subsequently, MPC and BMA were introduced *via* the RAFT polymerization method. Then, the hydrophobic OMe group was introduced to each hydroxyl group of the α-CD molecules. As a result, around 90% of the hydroxyl groups were successfully substituted by OMe groups. Fig. 2 shows the ^{1}H-NMR and FT-IR results of the synthesized OMe-PRX-PMB. Obviously, a strong OMe peak was observed at 3.2 and 3.3 ppm, which does not exist in PRX-PMB (Figure S3†). All the functional groups containing MPC units were successfully confirmed by combination of ^{1}H-NMR and FT-IR results. The detailed molecular profiles are summarized in Table 1.

3.2 Surface characterization of PRX block copolymer

The prepared polymer surfaces cast on the Cell Desk™ were analyzed by XPS. In all the cases of polymer surfaces, characteristic N_{1s} and P_{2p} signals from the PMB segment appeared at 402.5 eV and 134.0 eV, respectively, whereas the characteristic peak of the Cell Desk™ surface at 290 eV C_{1s} had disappeared (Fig. 3). This result indicates that all the polymer samples are uniformly prepared on the Cell Desk™ surface by means of the simple solvent cast method. Throughout an ellipsometry measurement, it was confirmed that all the polymer films were formed within a thickness of 20~30 nm (data not shown). In any case, it was confirmed that all the polymers were stably cast on the overall Cell Desk™ surface by anchoring the PMB segment.

The wettability of the prepared polymer surfaces was estimated in both air and water using water droplets and air bubbles, respectively. The contact angles of the air bubbles on the PMB, PRX-PMB, and OMe-PRX-PMB surfaces were not measured, because the air bubbles were rolling on these surfaces. These findings indicate that the surfaces are extremely hydrophilic in an aqueous environment and the contact angles are close to 0°. The contact angle hysteresis along with an air–water environmental change was indirectly measured by comparing both results (Fig. 4). The PMB surface showed a slightly higher contact angle hysteresis (~40°) than that of the Cell Desk™, which is possibly due to the increased directionality of the hydrophilic phosphorylcholine group in the water compared to the state in the air as previously reported.[28] The PEG-PMB and PRX-PMB surfaces showed a contact angle hysteresis of around 60°. It is thought that the swelling of the hydrophilic PEG and PRX segments of the block copolymer in the water was contributing to the slight increase of the contact angle hysteresis in addition to the directionality effect of the PMB segment. In contrast to the moderate hysteresis changes in these control samples, the OMe-PRX-PMB surface showed a contact angle hysteresis of around 100°. This indicates that the surface property of the OMe-PRX-PMB has drastically changed in response to the environmental change between air and water. The smoothness of all the surfaces was confirmed by atomic force microscope measurement, suggesting that the effect of surface roughness on the contact angle hysteresis should be negligible (Figure S4†). Even though more supporting information is required, we speculate that this dynamic change in the surface property is due to the dynamic movement of CD molecules on the PEG backbone.

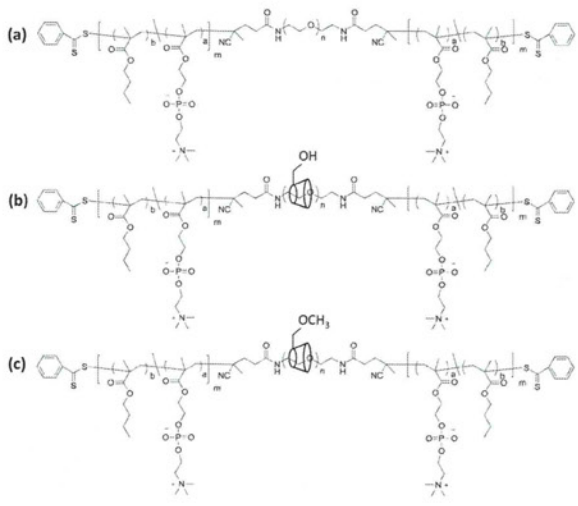

Fig. 1 Molecular structure of (a) PEG-PMB, (b) PRX-PMB, and (c) OMe-PRX-PMB.

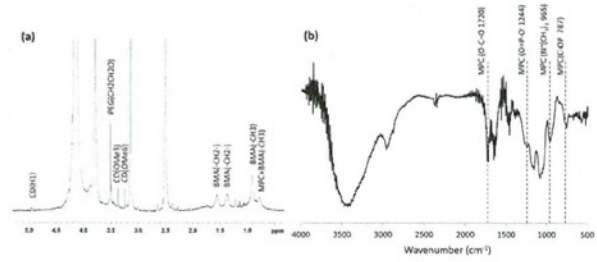

Fig. 2 (a) ^{1}H NMR (DMSO-d_6:MeOD = 1 : 1) and (b) FT-IR spectra of OMe-PRX-PMB.

To estimate the dynamic nature of the prepared PRX block copolymers in more detail, the surface dynamics in an aqueous media were estimated by the QCM-D measurement method as previously reported.[22] Generally, the energy dissipation value on a materials surface (ΔD) is directly related to the viscoelasticity of the materials adsorbed on an Au surface. When highly mobile surface elements such as tethering polymer chains or weakly cross-linked hydrogels exist, ΔD values drastically increase against rigid surfaces. This viscoelasticity of the surface could be interpreted as one of the parameters that indicate dynamic molecular movement of the surfaces. To consider the effect of the amount of polymers, each ΔD value was normalized to its adsorption mass related factor (Δf) using the following equation:

$$\text{Surface mobility factor } (M_f) = (D_{\text{sample, wet}} - D_{\text{gold, wet}})/(f_{\text{gold, dry}} - f_{\text{sample, dry}})$$

Table 1 Molecular profile of the synthesized polymers (^{1}H NMR)

	MPC (mol% in PMB)	BMA (mol% in PMB)	PEG (weight %)	Number of CD per PEG chain
Cell Desk™	0	0	0	0
PMB	19	81	0	0
PEG-PMB	23	77	24	0
PRX-PMB	12	88	23	12
OMe-PRX-PMB	12	88	23	12 methylation >90%

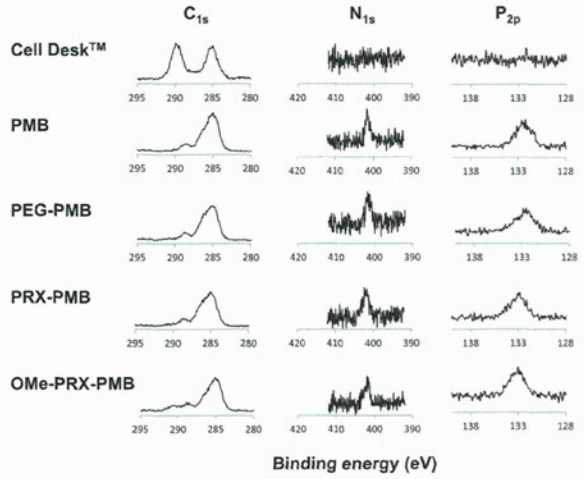

Fig. 3 XPS profile of cast polymer surfaces.

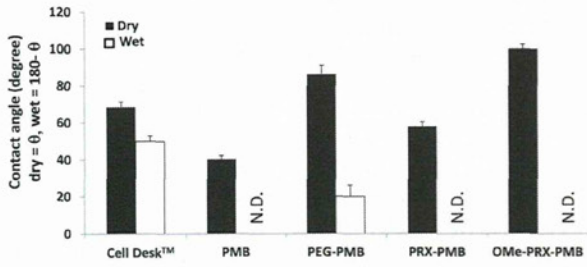

Fig. 4 Contact angles measured by water droplet in air and air bubble in water (n = 3).

Fig. 5 (a) shows the resulting value of M_f on each prepared polymer surface. The PEG-PMB showed a slightly higher M_f value than PMB. This is possibly due to the chain mobility of the hydrated loop-type PEG segment in the middle of the block copolymer. The OMe-PRX-PMB surface showed the highest M_f value among the prepared polymer surfaces, suggesting that the OMe group-containing the PRX segment exhibits the highest molecular mobility in an aqueous media. The lower M_f value on the PRX-PMB surface compared to those on the PEG-PMB and OMe-PRX-PMB surfaces is thought to be caused by the rigid crystalline formation of the CD molecules by intermolecular hydrogen bonding that interferes with the mobility of the PEG backbone. In any event, it was confirmed that the OMe-PRX-PMB surface exhibits the highest surface viscoelasticity—possibly induced by the dynamic molecular mobility on the surface—compared to other control polymer surfaces. Of special interest is the plot of the contact angle hysteresis along with the M_f value (Fig. 5 (b)). It is obvious that the relationship between the contact angle hysteresis and the M_f value is straightforward. This finding suggests that the dynamic change of surface wettability in response to the environmental change, is strongly governed by the molecular mobility on the surface.

3.3 Non-specific protein interaction with PRX block copolymer surfaces

Fig. 6 (a) shows the result of the human fibrinogen adsorption test. As expected, hydrophilic control samples (PMB, PEG-PMB, and PRX-PMB surfaces) showed relatively low fibrinogen adsorption. Similar results were also confirmed in the case of the

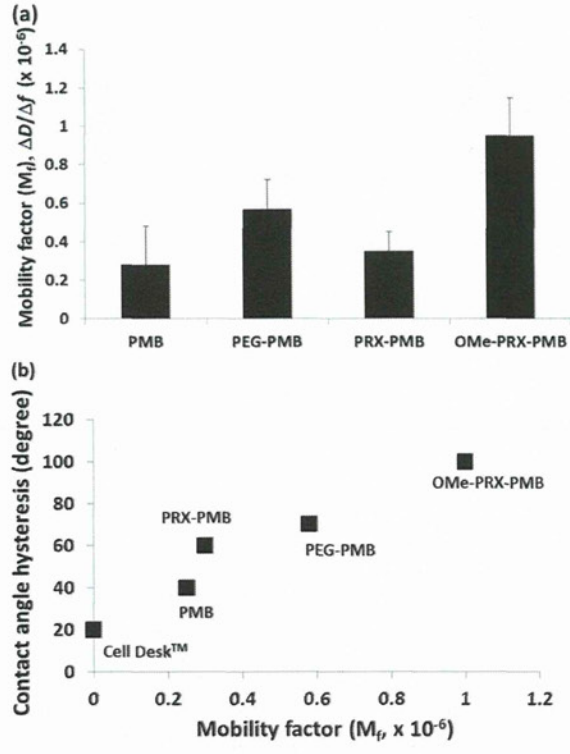

Fig. 5 (a) Result of M_f estimated from QCM-D and (b) plot of contact angle hysteresis *versus* M_f values (n = 3). The contact angle hysteresis was calculated by subtracting the contact angle of the water droplet in the air from that of the air bubble in the water bubble in water (n = 3).

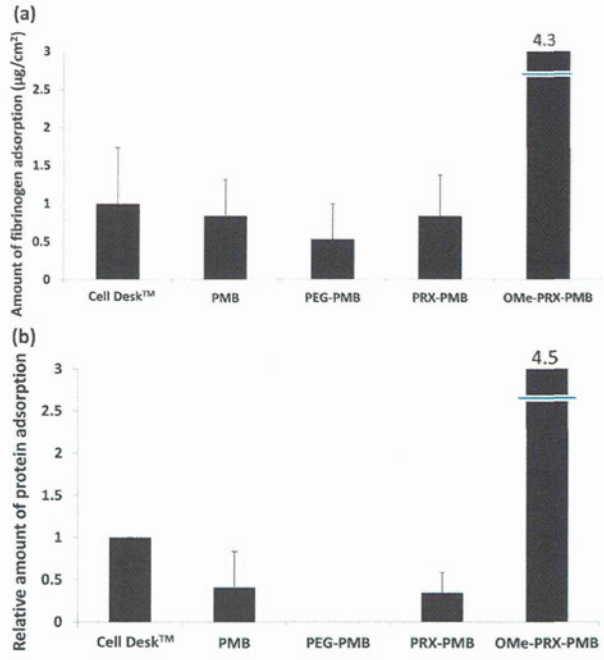

Fig. 6 Protein adsorption measured by micro-BCA™ method using (a) human fibrinogen at 10% plasma concentration and (b) 10% human PPP (n = 3).

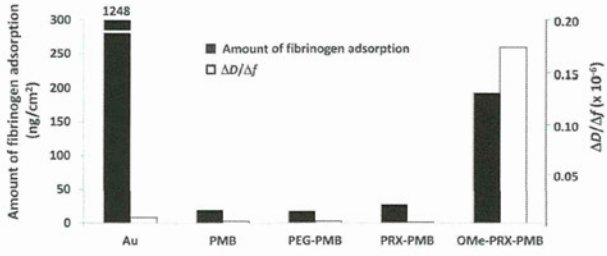

Fig. 7 Fibrinogen adsorption and $\Delta D/\Delta f$ value measured by QCM-D using 10% plasma concentration of human fibrinogen. Adsorption condition: flow rate = 0.1 mL min^{-1}, 1 h protein flow followed by 1 h PBS flow (pH 7.4).

whole human plasma adsorption test (Fig. 6 (b)). These results indicate that non-specific interaction between the hydrophilic control samples and the plasma protein was not very significant. In contrast, a significantly large amount of protein adsorption was observed on the OMe-PRX-PMB surface in both the fibrinogen and whole plasma adsorption test. Because the OMe-PRX-PMB surface exhibited an extremely hydrophilic nature in water (Fig. 4), the surface hydrophilicity in an aqueous environment could not explain this result. Even though the OMe are hydrophobic groups, they along with the rest of the polymer provide adequate enough hydrogen bonding to make the surface appear hydrophilic in aqueous media. However, these OMe groups exposed on the outermost surface still allow for contact with plasma proteins which leads to protein binding and accumulation.

To understand the state of the adsorbed proteins more clearly, fibrinogen adsorption was carried out by means of QCM-D under the flow adsorption condition. As a result, the adsorption behavior similar to that of micro-BCA™ was further confirmed on all the polymer surfaces (Fig. 7). In particular, a significantly large amount of fibrinogen adsorption was observed only on the hydrophobic Au and OMe-PRX-PMB surfaces. However, it is noteworthy that the state of adsorbed fibrinogen was quite different between the bare Au and OMe-PRX-PMB surfaces. In the case of the bare Au surface, the adsorbed fibrinogen molecules showed a very low $\Delta D/\Delta f$ value, which indicates that the state of the adsorbed fibrinogen molecules is very rigid because the interaction with the Au surface is quite strong. In contrast, the adsorbed fibrinogen on the OMe-PRX-PMB surface showed a significantly higher $\Delta D/\Delta f$ value. This indicates that the energy dissipation of the adsorbed fibrinogen molecules along with the micro-vibration of the substrates is quite high. This phenomenon is only observed when adsorbed substances weakly interact with the surface; that is, fibrinogen molecules are adsorbed on the OMe-PRX-PMB surface in quite a soft manner. Why this kind of soft interaction only occurred on the OMe-PRX surface is still unclear. However, taking into account the dynamic nature of the OMe-PRX-PMB surface (Fig. 4 and 5), it is plausible that the dynamically movable nature of the OMe-PRX-PMB surface is responsible for the soft interaction with the fibrinogen molecules. Namely, the strong interaction with the surface was disturbed by dynamic mobility of the surface, thus, adsorbed fibrinogen molecules were continuously vibrating along with the micro-vibration of the surfaces to induce high-energy dissipation.

The conformational change of adsorbed fibrinogen on the dynamic polymer surfaces was estimated by means of the ELISA test using two types of primary antibodies, 49D2 and clone2 G2. H9, which can specifically bind to the N-terminus of the α-chain (1–16 peptide sequence) and the C-terminus of the γ-chain (434–453 peptide sequence) of the adsorbed fibrinogen, respectively. Fibrinogen molecules have two specific binding motifs responsible for cellular adhesion and aggregation. One is the dodecapeptide sequence existing close to the C-terminus of the γ-chain (400–411 peptide sequence), which is a binding site to GPIIb/IIIa on the platelet to finally trigger the activation of the platelet.[29] The other motif consists of the two RGD sequences in the α-chain (RGDF and RGDS on 95–98 and 572–575 peptide sequence), which is a binding site to the GPIIb/IIIa of the platelets as well as the $\alpha_v\beta_3$ integrin on various cells.[30] Previous ELISA studies on the adsorbed fibrinogen on polymer surfaces demonstrated that the surface presentation of the dodecapeptide sequence in adsorbed fibrinogen on material surfaces was well correlated with platelet adhesion whereas the relation of the presentation of the RGD motifs with the platelet adhesion was not so clear.[31,32] These results indicate that the C-terminus of the γ-chain, presenting the dodecapeptide sequence in the fibrinogen, is essential to induce the platelet-fibrinogen interaction, and the N-terminus of the α-chain itself does not seem to have a significant effect on the platelet adhesion. Therefore, it is considered that the exposure level of the C-terminus of the γ-chain is a good parameter to estimate the potency of the platelet adhesion. Therefore, how well the appearance of the platelet GPIIb/IIIa binding site in the C-terminus γ chain is suppressed could be a key to the development of ideal blood-contacting materials. Fig. 8 (a) shows the quantitative result of the secondary antibody binding specifically to the primary antibody

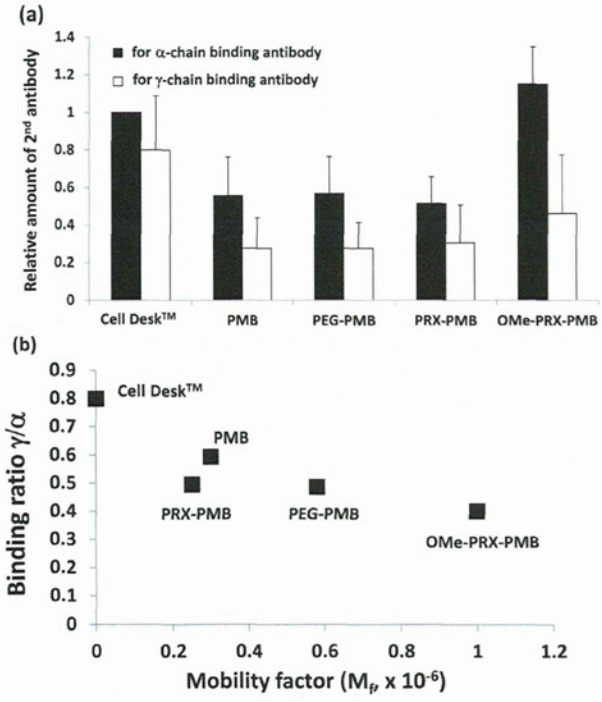

Fig. 8 (a) Relative amount of secondary antibody to the specific binding primary antibody on N-terminus α- and C-terminus γ-chains of adsorbed fibrinogen estimated by ELISA assay (n = 6) and (b) plot of γ : α binding ratio *versus* M_f values. Protein adsorption was carried out with 10% human plasma for 5 min contact prior to the ELISA test. The amount of secondary antibody was normalized to the amount of α-chain binding on the Cell Desk™.

bound to fibrinogen molecules. In the case of the Cell Desk™ surface, the amount of the binding antibody on both the γ- and α-chains was higher than that for other hydrophilic polymer surfaces, which indicates that the fibrinogen bound to the Cell Desk™ surface readily exposes both specific binding motifs. In contrast, other hydrophilic polymer surfaces showed a significantly lower level of the antibody binding in both the γ- and α-chains. This is possibly due to the quantitatively low level of adsorbed proteins as confirmed in the micro-BCA™ and QCM-D results. However, fibrinogen molecules on the OMe-PRX-PMB surface showed a quite interesting tendency. In spite of the significant amount of adsorbed plasma protein and fibrinogen, the amount of the secondary antibody for the C-terminus γ-chain binding antibody on the OMe-PRX-PMB surface was at a quite a low level compared to that on the Cell Desk™ surface (Figure S5†). This result suggests the possibility that inconsistent antibody binding was occurred due to the dynamic conformations which was induced by molecularly mobile segments in OMe-PRX-PMB. Fig. 8 (b) shows the plot of the antibody binding ratio (C-terminus γ-chain binding to N-terminus α-chain binding) *versus* the M_f values. It is obvious that the C-terminus γ-chain binding ratio compared to that of the N-terminus α-chain, decreased as the M_f value increased. Therefore, it is thought that the molecularly dynamic surfaces with high $\Delta D/\Delta f$ can induce moderate conformational changes no matter how many proteins are adsorbed on the surface.

3.4 Cellular responses to the PRX block copolymer surfaces

To estimate the effect of adsorbed plasma proteins on the biological responses, platelet and fibroblast adhesion tests were carried out by using the human PRP and NIH3T3 fibroblast. Fig. 9 (a) shows the result of platelet adhesion on the prepared polymer surfaces. Obviously, the Cell Desk™ surface induced large amounts of platelet adhesion on its surface, suggesting that the platelet adhesion is derived from a significant conformational change of the adsorbed proteins, including fibrinogen as confirmed by ELISA. In contrast, an insignificant number of adhering platelets was observed on all the prepared polymer surfaces. Fig. 9 (b) shows the quantitative result of adhering platelets along with the relative amount of the C-terminus γ-chain binding antibody. The resulting platelet adhesion was increased when the expression of the C-terminus γ-chain of the adsorbed fibrinogen was increased. This almost straightforward relationship is consistent with previously reported results.[31,32] The OMe-PRX-PMB surface showed a similar level of platelet adhesion in spite of the significant amount of adsorbed fibrinogen confirmed in the micro-BCA™ and QCM-D analyses. Several publications have stated that platelet adhesion normally increases in proportion to the amount of adsorbed fibrinogen.[33,34] However, the OMe-PRX-PMB surface showed a different tendency compared to those of the other materials surfaces. In particular, it is thought that the modulated conformational change of the adsorbed proteins, including fibrinogen on the dynamic OMe-PRX-PMB surface, can prevent platelet adhesion as discussed in Fig. 8 (b), in spite of the significant amounts of adsorbed proteins.

Fig. 10 (a) shows the resulting optical microscopic images of the polymer surfaces. Clearly, large numbers of fibroblasts were

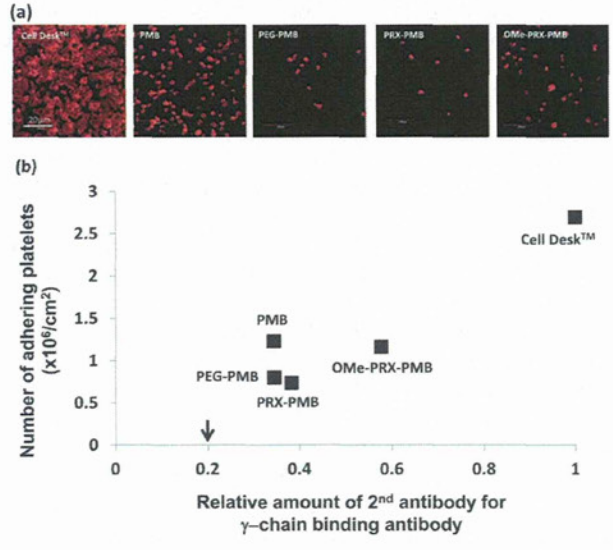

Fig. 9 (a) Fluorescent microscopic image of adhering platelets and (b) quantitative analysis of adhering platelets using LDH assay (n = 3). The plot also shows the relative amount of the secondary antibody for the C-terminus γ-chain binding antibody (normalized to the Cell Desk™). The arrow indicates the background level of ELISA. PRP contact was carried out for 3 h at 37 °C. Scale bar = 200 μm.

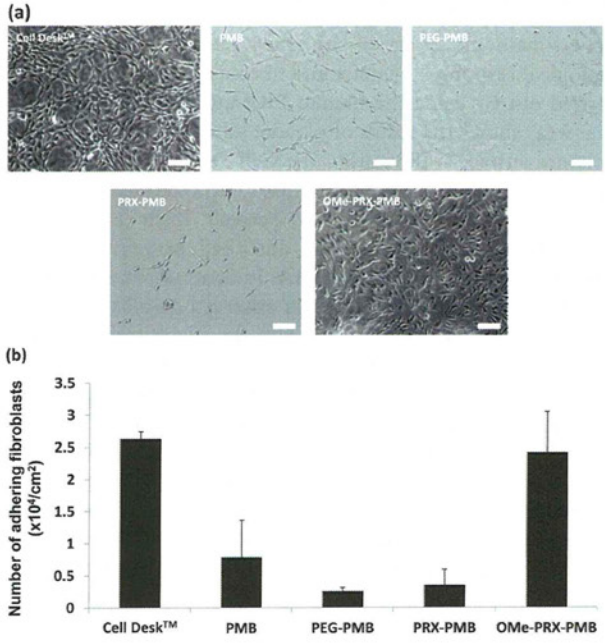

Fig. 10 (a) Optical microscopic images of adhering NIH3T3 fibroblasts and (b) the number of adhering cells. The initial cell concentration was 1.1×10^5 mL^{-1}. Scale bar = 100 μm.

adhering and proliferating on the Cell Desk™ surface, which indicates that surface adsorbed proteins undergo significant conformational changes to induce both platelet and fibroblast adhesion. On the other hydrophilic polymer surfaces, almost no adhering fibroblasts were observed. Because the amount of adsorbed proteins was quite low on the series of hydrophilic surfaces, it could be said that the prepared hydrophilic control samples do not induce significant non-specific interaction with the protein molecules; thus, platelet and cell adhesion was prevented. In contrast, the OMe-PRX-PMB surface showed a significant number of adhering fibroblasts (Fig. 10 (b)). Although the adhering level was slightly lower than that of the Cell Desk™ surface, a significant amount of adhesive and proliferated fibroblasts were also observed on the OMe-PRX-PMB surface. Taking into account the result of low platelet adhesion on the OMe-PRX-PMB surface, this cellular response seems out of the ordinary. Normal cell adhesive surfaces induce strong platelet responses as well because on these surfaces, not only fibrinogen and the von Willebrand factor but also other cell adhesive proteins such as fibronectin and vitronectin showed significant conformational changes to present most of their specific binding motifs to integrins.[35–37] In the case of adsorbed fibrinogen on the OMe-PRX-PMB surface, the amount of the secondary antibody for the C-terminus γ-chain binding antibody, which indicates the presentation of a specific binding site for platelet GPIIb/IIIa, was eliminated at a much lower level than that for the Cell Desk™. This was so, even though the amount of adsorbed proteins was at a much higher level than that for the Cell Desk™. Analyzing the presentation of integrin binding motifs in various cell adhesive proteins on OMe-PRX-PMB is now been undertaken and the result will be discussed in our forthcoming paper. Although the investigation has not yet concluded, we speculate that modulated conformational change of the cell adhesive proteins in serum could be one of the significant reasons that the OMe-PRX-PMB surface showed enhanced fibroblast adhesion in spite of eliminating platelet adhesion.

4. Conclusions

Dynamic OMe-PRX-PMB surfaces prepared by molecularly movable block copolymer induced specific biological responses by modulating the conformation of adsorbed proteins, especially fibrinogen. This finding is presumably related to the highly responsive dynamic properties of the OMe-PRX-PMB surface, which are characterized by the anomalous results of the contact angle hysteresis, the molecular mobility factor was determined by QCM-D, fibrinogen adsorption, and its conformational analyses. These results suggest that in such a molecularly movable surface, flexibly responds to a dynamic biological environment, and could be a promising way to design new biomaterials for regulating biological responses.

Acknowledgements

We thank Dr Tomo Ehashi and Dr Kwanwoo Nam for their helpful discussion on ELISA analysis, the cellular responses on the polymer surfaces, and AFM analysis.

References

1 J. Brash, T. Horbett, *ACS symposium series*, 343, American Chemical Society, Washington, D.C., 1987.
2 T. Horbett, J. Brash, *ACS symposium series*, 602, American Chemical Society, Washington, D.C., 1995.
3 D. Absolom, W. Zingg and A. Neumann, *J. Biomed. Mater. Res.*, 1987, **21**, 161.
4 T. R. Kyriakides, K. J. Leach, A. S. Hoffman and B. D. Ratner, *Proc. Natl. Acad. Sci. U. S. A.*, 1999, **96**, 4449.
5 H. Chen, L. Yuan, W. Song, Z. Wu and D. Li, *Prog. Polym. Sci.*, 2008, **33**, 1059.
6 M. Yamato, Y. Akiyama, J. Kobayashi, J. Yang, A. Kikuchi and T. Okano, *Prog. Polym. Sci.*, 2007, **32**, 1123.
7 P. Roach, D. Farrar and C. C. Perry, *J. Am. Chem. Soc.*, 2005, **127**, 8168.
8 K. Rechendorff, M. B. Hovgaard, V. P. Zhdanov and F. Besenbacher, *Langmuir*, 2006, **22**, 10885.
9 M. A. Cole, N. H. Voelcker, H. Thissen and H. J. Griesser, *Biomaterials*, 2009, **30**, 1827.
10 E. A. Vogler, *Biomaterials*, 2012, **33**, 1201.
11 T. Ooya, M. Eguchi and N. Yui, *J. Am. Chem. Soc.*, 2003, **125**, 13016.
12 N. Yui and T. Ooya, *Chem.–Eur. J.*, 2006, **12**, 6730.
13 H. Utsunomiya, R. Katoono, N. Yui, T. Sugiura, Y. Kubo, Y. Kato and A. Tsuji, *Macromol. Biosci.*, 2008, **8**, 655.
14 H. Hyun and N. Yui, *Macromol. Rapid Commun.*, 2011, **32**, 326.
15 H. Hyun and N. Yui, *Macromol. Biosci.*, 2011, **11**, 765.
16 T. Ooya, H. S. Choi, A. Yamashita, N. Yui, Y. Sugaya, A. Kano, A. Maruyama, H. Akita, K. Kogure and H. Harashima, *J. Am. Chem. Soc.*, 2006, **28**, 3852.
17 A. Yamashita, N. Yui, T. Ooya, A. Kano, A. Maruyama, H. Akita, K. Kogure and H. Harashima, *Nat. Protoc.*, 2006, **1**, 2861.
18 A. Yamashita, D. Kanda, R. Katoono, N. Yui, T. Ooya, A. Maruyama, H. Akita and H. Harashima, *J. Controlled Release*, 2008, **131**, 137.
19 Y. Yamada, T. Nomura, H. Harashima, A. Yamashita, R. Katoono and N. Yui, *Biol. Pharm. Bull.*, 2010, **33**, 1218.
20 Y. Yamada, M. Hashida, T. Nomura, H. Harashima, Y. Yamasaki, K. Kataoka, A. Yamashita, R. Katoono and N. Yui, *ChemPhysChem*, 2012, **13**, 1161.

21 Y. Yamada, T. Nomura, H. Harashima, A. Yamashita and N. Yui, *Biomaterials*, 2012, **33**, 3952.
22 Y. Inoue, L. Ye, K. Ishihara and N. Yui, *Colloids Surf., B*, 2012, **89**, 223.
23 Y. Mitsukami, M. S. Donovan, A. B. Lowe and C. L. McCormick, *Macromolecules*, 2001, **34**, 2248.
24 S. Zalipsky, C. Gilon and A. Zilkha, *Eur. Polym. J.*, 1983, **19**, 1177.
25 A. G. Hemmersam, K. Rechendorff, F. Besenbacher, B. Kasemo and D. S. Sutherland, *J. Phys. Chem. C*, 2008, **112**, 4180.
26 Y. Hong, S. H. Ye, A. Nieponice, L. Soletti, D. A. Vorp and W. R. Wagner, *Biomaterials*, 2009, **30**, 2457.
27 K. Ishihara, T. Ueda and N. Nakabayashi, *Polym. J.*, 1990, **22**, 355.
28 K. Futamura, R. Matsuno, T. Konno, M. Takai and K. Ishihara, *Langmuir*, 2008, **24**, 10340.
29 M. B. Gorbet and M. V. Sefton, *Biomaterials*, 2004, **25**, 5681.
30 J. M. Grunkemeier, W. B. Tsai, C. D. McFarland and T. A. Horbet, *Biomaterials*, 2000, **21**, 2243.
31 Y. Wu, F. I. Simonovsky, B. D. Ratner and T. A. Horbett, *J. Biomed. Mater. Res., Part A*, 2005, **74A**, 722.
32 W. B. Tsai, J. M. Grunkemeier and T. A. Horbett, *J. Biomed. Mater. Res.*, 2003, **67A**, 1255.
33 T. H. Fischer, H. S. Thatte, T. C. Nichols, D. E. Bender-Neal, D. A. Bellinger and J. N. Vournakis, *Biomaterials*, 2005, **26**, 5433.
34 B. Sivaraman and R. A. Latour, *Biomaterials*, 2010, **31**, 832.
35 A. M. Moulin, S. J. O'Shea, R. A. Badley, P. Doyle and M. E. Welland, *Langmuir*, 1999, **15**, 8776.
36 A. J. Garcia, M. D. Vega and D. Boettinger, *Mol. Biol. Cell.*, 1999, **10**, 785.
37 B. G. Keselowsky, D. M. Collard and A. J. Garcia, *J. Biomed. Mater. Res.*, 2003, **66A**, 247.

Biochemical and Biophysical Research Communications 424 (2012) 724–729

Contents lists available at SciVerse ScienceDirect

Biochemical and Biophysical Research Communications

journal homepage: www.elsevier.com/locate/ybbrc

Effects of both vitamin C and mechanical stimulation on improving the mechanical characteristics of regenerated cartilage

Seiji Omata [a,*], Shogo Sonokawa [b], Yoshinori Sawae [c], Teruo Murakami [d]

[a] Department of Biomedical Engineering, Graduate School of Biomedical Engineering, Tohoku University, Sendai, Miyagi, Japan
[b] Department of Mechanical Engineering, Graduate School of Engineering, Kyushu University, Fukuoka, Japan
[c] Department of Mechanical Engineering, Faculty of Engineering, Kyushu University, Fukuoka, Japan
[d] Advanced Biomaterials Division, Research Center for Advanced Biomechanics, Kyushu University, Fukuoka, Japan

ARTICLE INFO

Article history:
Received 22 June 2012
Available online 16 July 2012

Keywords:
Regenerated-cartilage tissue
Interconnection
Extracellular matrix network
Mechanical property
Mechanical stimulation

ABSTRACT

The present work describes the influence of both vitamin C (VC) and mechanical stimulation on development of the extracellular matrix (ECM) and improvement in mechanical properties of a chondrocyte–agarose construct in a regenerating tissue disease model of hyaline cartilage. We used primary bovine chondrocytes and two types of VC, ascorbic acid (AsA) as an acidic form and ascorbic acid 2-phosphate (A2P) as a non-acidic form, and applied uniaxial compressive strain to the tissue model using a purpose-built bioreactor. When added to the medium in free-swelling culture conditions, A2P downregulated development of ECM and suppressed improvement of the tangent modulus more than AsA. By contrast, application of mechanical stimulation to the construct both increased the tangent modulus more than the free-swelling group containing A2P and enhanced the ECM network of inner tissue to levels nearly as high as the free-swelling group containing AsA. Thus, mechanical stimulation and strain appears to enhance the supply of nutrients and improve the synthesis of ECM via mechanotransduction pathways of chondrocytes. Therefore, we suggest that mechanical stimulation is necessary for homogenous development of ECM in a cell-associated construct with a view to implantation of a large-sized articular cartilage defect.

1. Introduction

Articular cartilage covers the surface of the ends of bones in synovial capsules and performs the important function of high performance weight-bearing at very low friction and wear in daily activities during a healthy life. The behavior of articular cartilage tissue as a mechanical system is dependent chiefly on an extracellular matrix (ECM), which consists primarily of a protein, called type II collagen (10–20% of the wet weight), and proteoglycans (about 10% of the wet weight) [1]. Steric and electrostatic interactions of ECM molecules in the cartilage tissue occur between the cationic collagen fibers and the anionic proteoglycans to provide a highly charged environment under neutral pH conditions. Although adult articular cartilage is a remarkable load-bearing system, following traumatic injury or under conditions of wear and tear, it lacks the ability of self-repair, which can often lead to osteoarthritis (OA).

Such diseases of hyaline cartilage are a major health problem, especially in industrialized countries with relatively long active life expectancies. At present, no cell-assisted tissue regeneration therapy for the reliable and durable replacement of damaged articular cartilage has been established [2–4]. However, in recent years, tissue engineering has become a promising option for the treatment of OA and has allowed researchers to produce functional replacements for diseased cartilage [5,6]. Developments in therapeutic strategies for damaged cartilage treatment have increasingly focused on the promising technology of cell-assisted repair, which proposes the use of autologous chondrocytes or other cell types to regenerate articular cartilage [4,7].

There is still too little knowledge available to establish a suitable design strategy for reconstructing tissue-engineered cartilage that matches the mechanical properties of natural tissue. In this study, we focused on the relationship between the collagen network and the mechanical properties of a regenerated-cartilage tissue model and showed that the collagen network interconnecting chondrocytes improved the mechanical properties of the tissue to be equivalent to that of scaffold material without chondrocytes if there was no linkage between cells by the ECM network [8]. We used ascorbic acid (AsA), a type of vitamin C (VC), in the culture medium to control collagen synthesis in order to investigate the

* Corresponding author. Address: Sato-Huang/Deguchi Lab. Graduate School of Biomedical Engineering, Tohoku University, 6-6-1, Aoba, Aramaki, Aoba, Sendai, Miyagi 980-8579, Japan.
E-mail address: s_omata@bml.mech.tohoku.ac.jp (S. Omata).

0006-291X/$ - see front matter © 2012 Elsevier Inc. All rights reserved.
http://dx.doi.org/10.1016/j.bbrc.2012.07.019

effect of developing a collagen network on the mechanical properties of the tissue model. However, high concentrations of AsA were found to be toxic to the chondrocytes with no concomitant improvement in mechanical properties.

As for AsA above, we used ascorbic acid 2-phosphate (A2P), a non-acidic form, for suppressing the cytotoxicity and effective development of the mechanical characteristics of the tissue, and demonstrated the relationship between VCs in the culture medium and development of ECM and mechanical properties of the construct. In addition, we thought that applying a compressive deformation to the tissue model would not only improve diffusion of culture medium into the tissue and accelerate the supply of nutrients, but also activate cell-signaling via mechanosensor and mechanotransduction pathways. It is well known that loading mechanical stimuli to regenerated-cartilage tissue and chondrocytes is distinctly important for both enhancing synthesis of ECM and inducing chondrogenesis differentiation of stem cells [9]. Hence, in order to apply a compressive deformation to the tissue model for development of ECM, we made a purpose-built bioreactor capable of applying an uniaxial unconfined compressive strain to individual constructs in an incubator. The purpose of the present study was to investigate the effects of applying both two types of VC and dynamic compression to a regenerated-cartilage tissue model on the mechanical properties and development of the ECM network.

2. Materials and methods

2.1. Sample preparation and tissue culture

Primary bovine chondrocytes were isolated from metacarpophalangeal joints of steers purchased from a butchery using a sequential enzyme digestion method [10]. Full thickness articular cartilage tissue was harvested from the proximal articular surface of the metatarsal bone and finely diced with a scalpel. The finely diced cartilage tissue was enzymatically digested in a 25 unit/mL protease solution (P8811, Sigma, St Louis, MO) for 3 h and subsequently in a 200 unit/mL collagenase solution (C7657, Sigma) for 18 h at 37 °C. Both enzyme solutions were prepared in sterile tissue culture medium consisting of Dulbecco's modified Eagle's medium (DMEM; D5921, Sigma) supplemented with 20 v/v% Fetal Bovine Serum (FBS; 10437–028, Gibco, Carlsbad, CA), 2 mM L-glutamine (G7513, Wako Pure Chemical Industries, Ltd., Osaka, Japan), 100 unit/mL penicillin, 100 μg/mL streptomycin, 0.25 μg/mL amphotericin B (161–23181, Wako), 20 mM Hepes (H0887, Sigma), and 0.85 mM L-ascorbic acid (AsA; A5960, Sigma). The supernatant of the resultant solution was centrifuged to separate chondrocytes at 40 × g for 5 min. The resultant cell pellet was washed twice in fresh culture medium, and then cell number and cell viability were determined using Trypan Blue assay. In this study, Sigma Type VII agarose (A6560, Sigma) was used to prepare a chondrocyte–agarose construct. The agarose powder was dissolved in Earle's Balanced Salts Solution (EBSS; Sigma) at twice the required final concentration (1 w/v%) and mixed with an equal volume of the cell suspension to yield the desired agarose concentration with a final cell density of 1×10^7 cells/mL. The molten cell-agarose solution was poured into an acrylic mold and quenched into gel at 4 °C for 30 min to create cylindrical constructs with a diameter of 4 mm and a height of 2.5 mm. The resultant cell-agarose constructs were placed into a 24-well culture plate and cultured with 1 mL culture medium in an incubator at 37 °C and 5% CO_2. The culture medium was exchanged every 2 days. Several culture media with different VC concentrations, from 2.2 to 32 pmol/10^9 cells, were prepared and used to evaluate the effect of AsA and L-ascorbic acid 2-phosphate magnesium salt (A2P, Wako) concentrations. Culture medium without VC was also used as a control. Each medium is abbreviated as AsA(2.2), A2P(6.4), and A2P(32) hereafter in this paper.

After 1 day of free-swelling culture, the constructs in the experiment group were subjected to uniaxial compression within a purpose-built bioreactor system as shown in Fig. 1. The system permits the application of strain independently in both vertical and horizontal directions to individual constructs using a 24-well plate in a commercially available incubator. The movements were controlled with respective linear variable displacement transducers and linear guide actuators. Strain was applied to the individual constructs through a loading plate, which was attached to the actuator via a jig. Uniaxial cyclic compression up to a maximum amplitude of 15% was applied in a triangular waveform at a frequency of 1 Hz for 6 h and subsequently off-loaded with the plate resting for each construct over the subsequent 18 h. Control constructs were cultured, in contrast, with both upper and lower plates for diffusion through the sides alone.

2.2. Measurement of mechanical property

To examine the influence of VC concentration, cell-agarose constructs were subjected to unconfined compression while immersed in culture medium at room temperature. Individual constructs were tested after culture periods of 22 days. Mechanical tests were

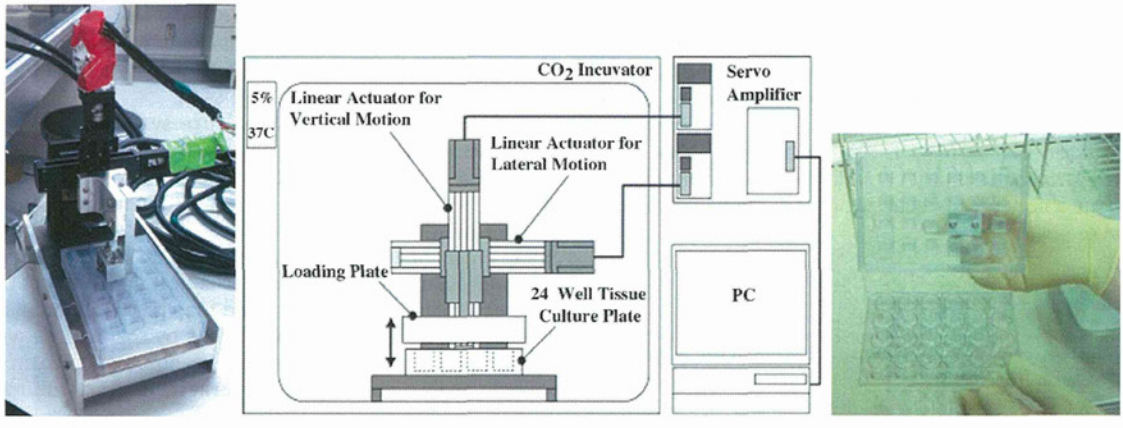

Fig. 1. Photograph (left) and Schematic drawing (center) of mechanical loading system mounted within tissue culture incubator. Loading plate with 22 plungers coupled with a 24-well culture plate (right).

performed with an impermeable stainless steel plunger at a strain rate of 0.5 mm/min up to a strain of 10%, while the load was recorded with a 10 N load sensor. The tangent modulus of the construct was calculated from the slope of a straight-line approximation of the stress–strain curve with a range of 0–15% strain using the least-square method.

2.3. Immunohistology

Separate constructs were used for trichrome immunofluorescence observation to examine the morphological characteristics of the elaborated ECMs, in particular type I collagen, type II collagen and chondroitin sulfate. After the prescribed culture periods, representative constructs were cut into slices with a thickness of approximately 1 mm using a knife. The slices were washed in PBS(−) and subsequently incubated in PBS(−) + 1 w/v% bovine serum albumin (BSA; Wako) for 30 min at 37 °C. These slices were incubated in PBS(−) containing the three monoclonal antibodies (bovine IgG1 isotype anti-type I collagen, Funakoshi, Tokyo, Japan; embryonic chicken IgG2a isotype anti-type II collagen, Funakoshi; mouse IgM isotype anti-chondroitin sulfate, Sigma) for 90 min at 37 °C to primarily label the collagens and the proteoglycan at once. The slices were then washed three times in PBS(−) for 10 min and incubated in PBS(−) containing the three secondary antibodies corresponding to each of the primary antibodies (Alexafluor 350-conjugated anti-mouse IgG1 antibody, A21120; Alexafluor 488-conjugated anti-mouse IgG2a antibody, A11001; Alexafluor 568-conjugated anti-mouse IgM antibody, A21043, Invitrogen) for 60 min at 37 °C. Labeled ECM molecules were fluorescently visualized within the cultured cell-agarose construct. The fluorescently stained specimens were mounted on the coverslip and observed using a confocal laser scanning microscope (CLSM; Eclipse; Nikon Corp., Tokyo, Japan).

2.4. Cell viability

The cell viability of individual constructs was assessed at different concentration of the VCs using a previously reported protocol [11]. The cultured constructs were cut into slices with a thickness of approximately 1 mm and washed in PBS(−) for 5 min at 37 °C. These slices were incubated in PBS(−) containing two fluorescent dyes (live cells: Calcein AM, Molecular Probes; dead cells: Ethidium homodimer-1, Molecular Probes) for 15 min at 37 °C. The fluorescently stained constructs were then washed by PBS(−) several times and mounted on the coverslip and observed by CLSM.

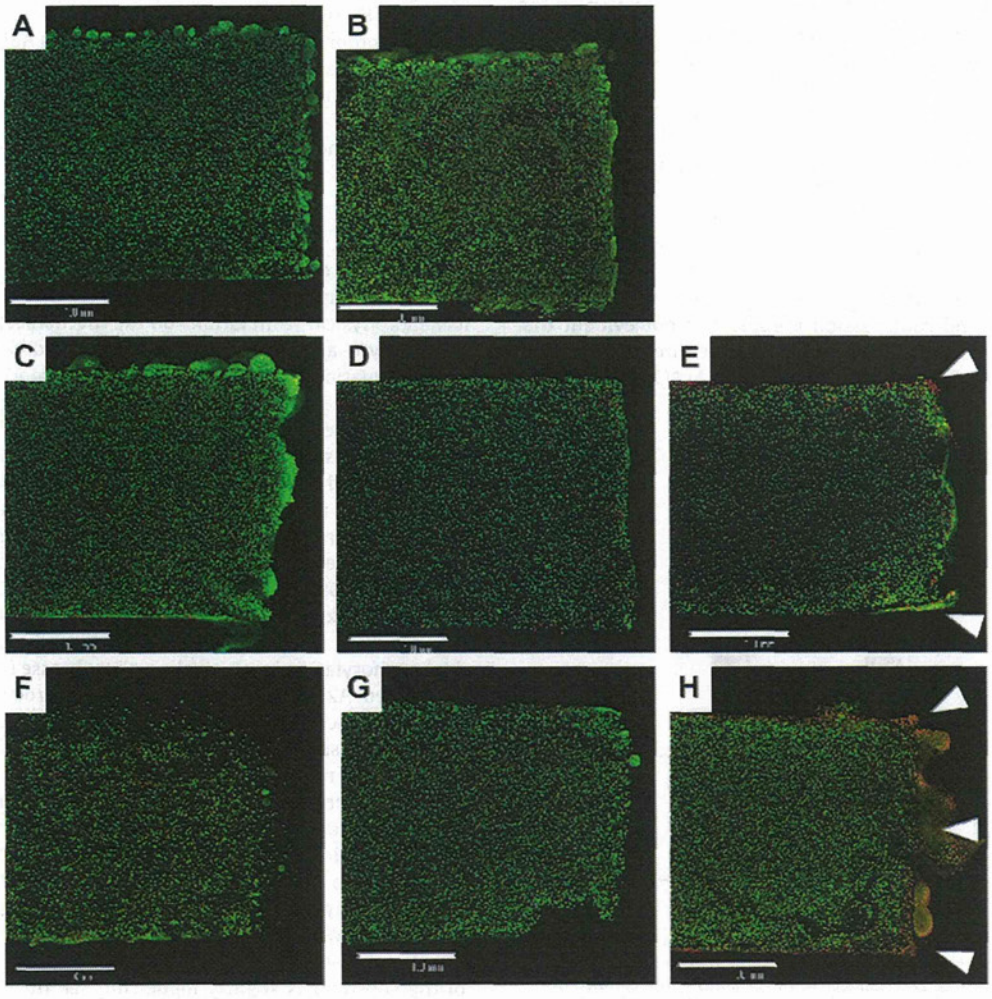

Fig. 2. Low-magnification immunofluorescence images of cell viability under free swelling (A, B, C, F), control (D, G) or compression (E, H) culture conditions. (A): without VC; (B): AsA(2.2); (C–E): A2P(6.4); (F–G): A2P(32). Green represents live cells and red represents dead cells. The culture period was 22 days. Each trichrome-stained sample represents an individual culture. The scale bar represents 1 mm.

2.5. Statistical analysis

Result of the tangent modulus were expressed as the mean ± sample standard deviation (*SD*). The significance of the difference between each experimental group was assayed using the two-tailed Welch's *t*-test. The degree of freedom was abbreviated to *df*. If the results of pairwise comparisons between two groups were *P*-value < 0.01, $d > 1$ and $(1 - \beta) > 0.8$ simultaneously, we judged the difference as significant in the tangent modulus, where *P*-value: level of significance; *d*: Cohen's *d*, an indicator of the effect size [12]; $(1 - \beta)$: the power of the test calculated by R language.

3. Results

3.1. Viability test

In the majority of cases there was a high degree of viability after 22 days of culture, as indicated in Fig. 2. However, some cytotoxicity was evident in the corner of the constructs in two experimental groups, namely A2P(6.4), and most particularly A2P(32), as indicated by the arrow-heads in Fig. 2(E) and (H).

3.2. Measurement of mechanical properties

To evaluate the influence of the mechanical stimulation on the cultured constructs, the tangent moduli of each group after 22 days of culture is shown in Fig. 3. Comparison within the four free-swelling groups only indicated significant differences between the without VC and the AsA(2.2) groups, the latter revealing an increased tangent modulus. By applying cyclic compression to the construct with addition of VC to the culture medium, there was not a clear difference between free-swelling and compression groups for AsA. By contrast, both tangent moduli of the two compression groups were higher than those of several free-swelling samples in each A2P dose group (A2P(6.4) and A2P(32)). Each tangent modulus of the control groups with A2P was ranked against the free-swelling and compression groups. It is not evident that there were differences between each pair of the three compression groups (AsA(2.2), A2P(6.4) and A2P(32)) (AsA(2.2), A2P(6.4): $df = 16$, $P = 0.47$, $d = 0.32$, $(1 - \beta) = 0.030$), but A2P(32) was lower than both AsA(2.2) and A2P(6.4) because each effect size (d) was large but each power ($(1 - \beta)$) was not (AsA(2.2), A2P(32): $df = 25$, $P = 0.017$, $d = 0.99$, $(1 - \beta) = 0.43$; A2P(6.4), A2P(32): $df = 15$, $P = 0.011$, $d = 1.3$, $(1 - \beta) = 0.54$).

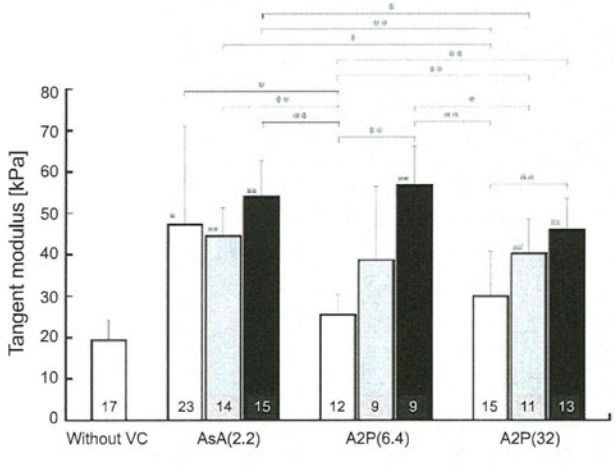

Fig. 3. Comparison of the tangent moduli after 22-day culture period. Cultures were terminated following free-swelling (white column), control (gray), or compression (black) conditions. Each number in the columns is the cultured sample number and each sample represents an individual culture. The error bar represents SD. Sharps (# and ##) and asterisks (* and **) show respective statistical significance between control group and each groups in Welch's *t*-test. #, *: $d > 1$, $P < 0.01$, $(1 - \beta) > 0.8$; ##, **: $d > 2$, $P < 0.01$, $(1 - \beta) > 0.8$.

3.3. Histological observation

Fig. 4 shows immunofluorescent images at low and high magnification revealing the ECM distribution (type I and II collagen and chondroitin sulfate) after 22 days. The high-magnification images were taken in the vicinity of the center of the construct. As indicated in Fig. 4(a) and (A), it is clear that with the absence of VC in the culture medium, there was only a limited amount of ECM. By contrast, in the free-swelling group (AsA(2.2)), there was a fairly uniform distribution of ECM across the construct (Fig. 4(b)). As indicated by the arrows in Fig. 4(B), at high magnification, this revealed a collagen network interconnected between chondrocytes. The low-magnification images for each of the A2P dose groups revealed a similar distribution in ECM across the constructs (Fig. 4(c)–(h)), although it was difficult to observe the ECM in the peripheral region of the compressed construct associated with group A2P(32), as indicated by the arrow-heads in Fig. 4(h). In the high magnification images, type II collagen seems to be interconnected between the chondrocytes, as indicated by the arrow in Figs. 4(E), (G) and (H). However, those examinations revealed that the compression groups of A2P(6.4) and A2P(32) were associated with a more abundant collagen network than the corresponding free-swelling groups. In addition, it is clearly evident that the distribution of chondroitin sulfate is restricted to the peripheral regions of the chondrocytes.

4. Discussion

In order to establish a suitable method for regenerating tissue-engineered cartilage, we studied the effects of two types of chemical and physical stimulations on the mechanical properties of the chondrocyte–agarose construct a regenerated-cartilage model. The first stimulation was the addition of high concentration of VC to the culture medium in order to enhance collagen synthesis. The second was the application of a compressive strain to the construct using a purpose-built bioreactor. Our results show that compressive strain had led to an increase in the tangent modulus and that the collagen network had become dense and interconnected among chondrocytes. We have already described the importance of chondrocyte linkage by ECM for the development of bulk elasticity of the construct in a previous study.

It is well known that even though A2P has no physiological activity, it can nevertheless reproduce the effect of VC activity after dephosphorylation by an alkaline phosphatase (ALP) [13]. Dephosphorylated A2P, or AsA, penetrates chondrocytes through a VC transporter, chiefly the sodium-dependent VC transporter 2 (SVCT2), and supports collagen synthesis as a cofactor in the rough endoplasmic reticulum [14]. In free-swelling culture conditions, we only observed a small number of collagen molecules distributed in the construct. We also observed that the tangent moduli of both A2P dose groups were lower than the moduli of AsA(2.2). We must also consider the reaction rates of both dephosphorylation of A2P by ALP and the transport of AsA into the cytosol via SVCT2. The Michaelis constants of bovine chondrocytes ALP and SVCT2 are 1–10 and 62 ± 25 μM, respectively [15,16]. The affinity of the substrate is slightly higher for ALP than for SVCT2, and as a result, AsA concentration around chondrocytes was lower in the A2P group. The rate of collagen synthesis was also relatively lower in the A2P group than the AsA dose group. Hence, the

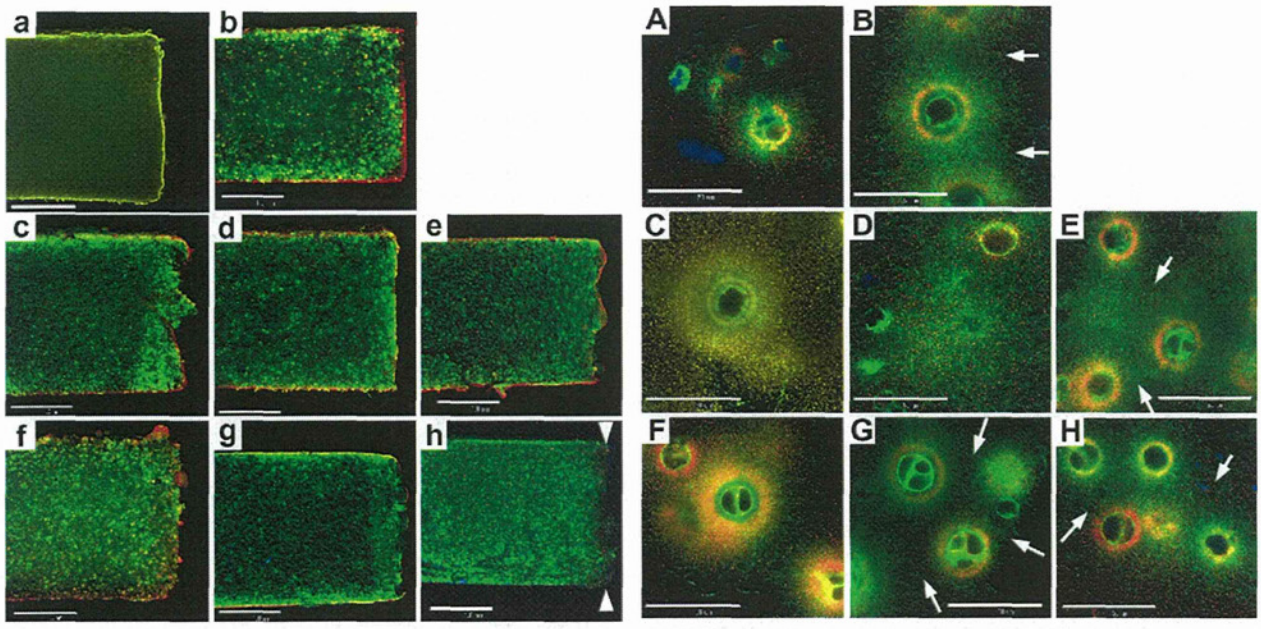

Fig. 4. Low- and high-magnification immunofluorescence images of ECMs under either free-swelling (a, b, c, f, A, B, C, F), control (d, g, D, G), or compression (e, h, E, H) culture conditions. (a, A): without VC; (b, B): AsA(2.2); (c–e, C–E): A2P(6.4); (f–g, F–G): A2P(32). Blue: type I collagen; green: type II collagen; red: chondroitin sulfate. The culture period was 22 days. Scale bars represent 1 mm (a–g) and 50 μm (A–G), respectively. Arrow-heads indicate that we could not observe ECMs at periphery of the tissue of compression group A2P(32). Arrows indicate interconnections among chondrocytes by type II collagen network.

tangent modulus of the free-swelling groups with A2P was suppressed by restraining cytotoxicity of AsA.

When applying compressive strain to the construct, each tangent modulus of A2P(6.4) and A2P(32) was higher than the moduli for the respective free-swelling groups. This is because the collagen network of these groups expanded, which allowed collagen fibers to interconnect among the chondrocytes. We think this mechanical stimulation enhanced diffusion of A2P and nutrients, homogenizing A2P within the construct. In addition, the stimulation probably excited a mechanosensor, activating cell-signaling pathways, namely the mechanotransduction pathways. It is well-known that mechanical stimulation causes chondrocytes to undergo several biological responses involving cartilage remodeling strategies that are relevant to the implantation of cultured tissue [17], e.g., activation of a mitogen-activated protein kinase (MAPK) pathway, a cell-signaling pathway [18,19], an increase in GAG biosynthesis [20], and regulation of inflammatory species synthesis [21]. These chondrocyte responses followed soon after mechanical stimulation and activity of the MAPK pathway was maintained for 5–60 min [18,19]. In synthesizing ECM with mechanical stimulation, chondrocytes built up the collagen network and adapted to changes in the deformation around the cells. Therefore, the compression group with A2P had a higher tangent modulus than the free-swelling group.

The tangent modulus of the compression group with A2P(32) tended to decrease more than the compression group of A2P(6.4) because ECM had been less developed in the peripheral region of A2P(32) than A2P(6.4). Moreover, viability observations revealed that cytotoxicity occurred at the peripheral regions of A2P(32). Generally, we can think that uniaxial compressive deformation of a cylinder model follows the same physics as two-dimensional tension in a plane perpendicular to the axial direction. When the tangent modulus is uniform in the construct, the force at the outer diameter position will be the largest because a reactive force is directly proportionate to the radius. Therefore, less ECM at the peripheral region induced a decrease in the tangent modulus of the construct.

As mentioned above, it is not easy to homogenously develop ECM in free-swelling culture conditions for the purpose of making large-sized regenerated-cartilage tissue. Based on the results of this study, it is necessary to apply mechanical strain to the construct because nutrients should be uniformly supplied. If we also consider the diffusion of nutrients under free-swelling culture conditions, we must note that the diffusion coefficient of water in agarose gel is about $10 \times 10^{-10}\ m^2s$ [22,23]. Applying Fick's law, this means that a water molecule diffuses 10 mm per day in the gel. Pluen et al. reported that the diffusion coefficients of proteins in 0.1 M PBS(−) solution, lactalbumin and ovalbumin, were 0.8–$1 \times 10^{-10}\ m^2s$ [24], and therefore that nutrient particles diffuse 3 mm per day in the gel. Moreover, if the ECM of the cultured construct is dense, it is difficult for nutrients to diffuse in the tissue and the diffusion coefficient will be decreased. Thus, for clinical implantation of a large-sized regenerated-cartilage tissue in order to treat a cartilage defect, the construct should be prepared by applying mechanical stimulation, which would homogenously develop the ECM network.

In summary, this study investigated the influence of two types of VC, AsA and A2P, on the development of the ECM network and regulation of the mechanical properties of chondrocyte–agarose constructs. The collagen network of A2P dose groups improved more than the AsA dose group in free-swelling culture conditions and the tangent modulus of the A2P dose groups did not increase. Moreover, it is clear that free-swelling culture conditions suppressed development of ECM of the inner tissue more than the outer tissue. When applying compressive strain to the construct, tangent moduli of the A2P dose groups were higher due to the fact that ECM networks of the inner tissue had been upregulated with interconnections among the chondrocytes. Additionally, we propose that mechanical stimulation enhanced diffusion of nutrients and improved synthesis of the ECM via mechanotransduction

pathways. We conclude that the application of mechanical stimulation to a large-sized engineered-tissue is necessary for the treatment of articular cartilage defects of various sizes and forms.

Acknowledgments

This study was financially supported by the Grant-in-Aid for Scientific Research from the Japan Society for the Promotion of Science (20360078).

References

[1] R.M. Schulz, A. Bader, Cartilage tissue engineering and bioreactor systems for the cultivation and stimulation of chondrocytes, Eur. Biophys. J. 35 (2007) 539–568.
[2] A. Getgood, R. Brooks, L. Fortier, N. Rushton, Articular cartilage tissue engineering: today's research, tomorrow's practice?, J Bone Joint Surg. Br. 91 (2009) 565–576.
[3] S.R. Frenkel, P.E. Di Cesare, Scaffolds for articular cartilage repair, Ann. Biomed. Eng. 32 (1) (January 2004) 26–34.
[4] J. Farr, B. Cole, A. Dhawan, J. Kercher, S. Sherman, Clinical cartilage restoration: Evolution and overview, Clin. Orthop. Relat. Res. 469 (2011) 2696–2705.
[5] A.H. Gomoll, G. Filardo, L. de Girolamo, J. Esprequeira-Mendes, M. Marcacci, W.G. Rodkey, R.J. Steadman, S. Zaffagnini, E. Kon, Surgical treatment for early osteoarthritis. part I: cartilage repair procedures, Knee Surg. Sports Traumatol. Arthrosc. 20 (2012) 450–466.
[6] A.H. Gomoll, G. Filardo, F.K. Almqvist, W.D. Bugbee, M. Jelic, J.C. Monllau, G. Puddu, W.G. Rodkey, P. Verdonk, R. Verdonk, S. Zaffagnini, M. Marcacci, Surgical treatment for early osteoarthritis. part II: allografts and concurrent procedures, Knee Surg. Sports Traumatol. Arthrosc. 20 (2012) 468–486.
[7] C.M. Revell, K.A. Athanasiou, Success rates and immunologic responses of autogenic, allogenic, and xenogenic treatments to repair articular cartilage defects, Tissue Eng. Part B 15 (2009) 1–15.
[8] S. Omata, Y. Sawae, T. Murakami, Influence of ascorbic acid (asa) concentration in culture medium on mechanical property of regenerated cartilage, J. Environ. Eng. 6 (2011) 416–425.
[9] S. Grad, D. Eglin, M. Alini, M.J. Stoddart, Physical stimulation of chondrogenic cells in vitro: A review, Clin. Orthop. Relat. Res. 469 (2011) 2764–2772.
[10] D.A. Lee, D.L. Bader, Compressive strains at physiological frequencies influence the metabolism of chondrocytes seeded in agarose, J. Orthop. Res. 15 (1997) 181–188.
[11] M.M. Knight, S.R. Roberts, D.A. Lee, D.L. Bader, Live cell imaging using confocal microscopy induces intracellular calcium transients and cell death, Am. J. Physiol. Cell Physiol. 284 (2003) 1083–1089.
[12] J. Cohen, Statistical power analysis for the behavioral sciences, 2nd ed., Lawrence Erlbaum Assoc Inc., New Jersey, 1988.
[13] S. Takamizawa, Y. Maehata, K. Imai, H. Senoo, S. Sato, R. Hata, Effects of ascorbic acid and ascorbic acid 2-phosphate, a long-acting vitamin C derivative, on the proliferation and differentiation of human osteoblast-like cells, Cell Biol. Int. 27 (2004) 255–262.
[14] I. Savini, A. Rossi, C. Pierro, L. Avigliano, M.V. Catani, SVCT1 and SVCT2: key proteins for vitamin C uptake, Amino Acids 34 (2008) 347–355.
[15] A.L. McNulty, T.P. Vail, V.B. Kraus, Chondrocytenext term transport and concentration of ascorbic acid is mediated by SVCT2, Biochim. Biophys. Acta 1712 (2005) 212–221.
[16] R. Fortuna, H.C. Anderson, R.P. Carty, S.W. Sajdera, Enzymatic characterization of the chondrocytic alkaline phosphatase isolated from bovine fetal epiphyseal cartilage, Biochim. Biophys. Acta 570 (1979) 291–302.
[17] L. Ramage, G. Nuki, D.M. Salter, Signalling cascades in mechanotransduction: cell-matrix interactions and mechanical loading, Scand. J. Med. Sci. Sports 19 (2009) 457–469.
[18] J.B. Fitzgerald, M. Jin, D. Dean, D.J. Wood, M.H. Zheng, A.J. Grodzinsky, Mechanical compression of cartilage explants induces multiple time-dependent gene expression patterns and involves intracellular calcium and cyclic AMP, J. Biol. Chem. 279 (2004) 19502–19511.
[19] J.B. Fitzgerald, M. Jin, D.H. Chai, P. Siparsky, P. Fanning, A.J. Grodzinsky, Shear- and compressioninduced chondrocyte transcription requires MAPK activation in cartilage explants, J. Biol. Chem. 283 (2008) 6735–6743.
[20] J.D. Kisiday, J.H. Lee, P.N. Siparsky, D.D. Frisbie, C.R. Flannery, J.D. Sandy, A.J. Grodzinsky, Catabolic responses of chondrocyte-seeded peptide hydrogel to dynamic compression, Ann. Biomed. Eng. 37 (2009) 1368–1375.
[21] O.O. Akanji, P. Sakthithasan, D.M. Salter, T.T. Chowdhury, Dynamic compression alters NFκB activation and IκB-α expression in IL-1β-stimulated chondrocyte/agarose constructs, Inflamm. Res. 59 (2010) 41–52.
[22] E. Davies, Y. Huang, J.B. Harper, J.M. Hook, D.S. Thomas, I.M. Burgar, P.J. Lillford, Dynamics of water in agar gels studied using low and high resolution 1H NMR spectroscopy, Int. J. Food Sci. Technol. 45 (2010) 2502–2507.
[23] N.O. Gustafsson, B. Westrin, A. Axelsson, G. Zacchi, Measurement of diffusion coefficients in gels using holographic laser interferometry, Biotechnol. Progr. 9 (1993) 436–441.
[24] A. Pluen, P.A. Netti, R.K. Jain, D.A. Berk, Diffusion of macromolecules in agarose gels: comparison of linear and globular configurations, Biophys. J. 77 (1999) 542–552.

Proceedings of the Institution of Mechanical Engineers, Part J: Journal of Engineering Tribology
http://pij.sagepub.com/

Importance of adaptive multimode lubrication mechanism in natural and artificial joints

Teruo Murakami

Proceedings of the Institution of Mechanical Engineers, Part J: Journal of Engineering Tribology 2012 226: 827 originally published online 28 June 2012
DOI: 10.1177/1350650112451377

The online version of this article can be found at:
http://pij.sagepub.com/content/226/10/827

Published by:
SAGE
http://www.sagepublications.com

On behalf of:
Institution of Mechanical Engineers
Institution of MECHANICAL ENGINEERS

Original Article

Institution of MECHANICAL ENGINEERS

Journal of ENGINEERING TRIBOLOGY

Proc IMechE Part J:
J Engineering Tribology
226(10) 827–837

DOI: 10.1177/1350650112451377
pij.sagepub.com

SAGE

Importance of adaptive multimode lubrication mechanism in natural and artificial joints

Teruo Murakami[1,2]

Abstract

The healthy natural synovial joints maintain excellent load-carrying capacity and lubricating properties with extremely low friction and minimum wear even under heavily loaded conditions. The superior lubricating performance appears to be actualized by not single lubrication mode but the synergistic combination of various modes depending on the severity of operating conditions. This mechanism is called adaptive multimode lubrication and the application of this good working lubrication mechanism to artificial joints with soft layer is expected to contribute to remarkable improvement in longevity of joint prostheses. However, some of detailed mechanisms in natural synovial joints have not yet been clarified. In this article, the effectiveness of biphasic lubrication in natural synovial joints was examined by biphasic finite element analysis under both the on–off loading (migrating contact) and the continuous loading (continuous contact) to cartilage. Then, the method to suppress the gradual rising in friction for articular cartilage under the continuous loading is discussed. Finally, the effectiveness of fibre reinforcement in hydrogel artificial cartilage was examined in walking simulator test.

Keywords

Biotribology, natural synovial joints, articular cartilage, artificial joints, artificial cartilage, adaptive multimode lubrication

Date received: 17 October 2011; accepted: 15 May 2012

Introduction

Application of joint replacements to patients with osteoarthritis or rheumatoid arthritis brings the recovery of walking ability and relief from severe pain. However, in certain cases of artificial joints composed of ultrahigh molecular weight polyethylene (UHMWPE) and metal or ceramic components, the revision operations are conducted due to the loosening of joint prostheses which is usually derived from wear debris induced osteolysis.[1,2] Therefore, the reduction of wear is strongly required for improvement in the longevity of artificial joints. In contrast, healthy natural synovial joints maintain very low friction and minimum wear for a long life, although some performances may be reduced by cartilage deterioration due to ageing. To establish low friction and low wear in artificial joints, we should elucidate the synergistic lubrication mechanism in natural synovial joints and then apply the effective lubrication mechanisms to artificial joint systems. In this article, the adaptive multimode lubrication mechanism[3] and related phenomena in natural synovial joints are first described. Then, the biphasic finite element (FE) analyses for reciprocating sliding of articular cartilage are conducted under both the on–off loading and the continuous loading conditions. Next, the effective method to inhibit an increase in friction for sliding pair of articular cartilage and glass plate in repeated reciprocating tests under continuous loading condition is discussed. Subsequently, the improvement of lubrication performance in joint prostheses with compliant artificial cartilage is exhibited.

The first aim of this article is the elucidation of adaptive multimode lubrication mechanism in natural synovial joints, particularly from viewpoints of the biphasic lubrication considering loading conditions and the adsorbed film formation considering roles of lubricant constituents. The second aim is the evaluation of effectiveness in the application of superior lubrication mechanism in articular cartilage to artificial hydrogel cartilage in simulator test.

[1]Department of Mechanical Engineering, Kyushu University, Fukuoka, Japan
[2]Research Center for Advanced Biomechanics, Kyushu University, Fukuoka, Japan

Corresponding author:
Teruo Murakami, Research Center for Advanced Biomechanics, Kyushu University, Motooka, Fukuoka 819-0395, Japan.
Email: tmura@mech.kyushu-u.ac.jp

Adaptive multimode lubrication in natural synovial joints

The healthy synovial joints maintain excellent load-carrying capacity and lubricating properties with extremely low friction and minimum wear even under heavily loaded conditions in hip, knee and ankle joints. This superior lubricating performance appears to be actualized by not a single lubrication mode but the synergistic combination of various modes from the fluid film lubrication to boundary lubrication corresponding to the severity of rubbing conditions, as pointed out by Dowson.[4] He described that the major lubrication mechanism would seem to be some form of elastohydrodynamic action determined by sliding or squeeze film action between porous surfaces with boundary lubrication providing the surface protection in cases of severe loading and little movement.

The author first focused on the influence of elastic soft layer of articular cartilage on lubrication in natural joints. In the previous study using pendulum tester, the frictional behaviours were investigated for two-dimensional cylindrical hip joint models with and without 3 mm soft layer prepared as radial clearance of 0.1 mm for concave cup specimen with a radius of 25 mm.[5] To observe simultaneously the changes in contact conditions and amplitude of swing, the photoelastic method was applied, where epoxy resin with Young's modulus of 3.0 GPa was used approximately for elastic subchondral and cancellous bone model and polyurethane with Young's modulus of 10 MPa as soft layer corresponding to articular cartilage. The swing behaviours immediately after loading of 10 N/mm lubricated with paraffinic oil indicated that the joint model without soft layer shows rapid damping, i.e. high friction. In contrast, the existence of soft layer reduced the friction due to elastohydrodynamic lubrication (EHL) mechanism with enlarged contact zone. The average friction coefficients were estimated as 0.03–0.04 for model with soft layer, and 0.12 for model without soft layer for lubricant viscosity of 0.056 Pa s. Thus, the friction coefficient for low-viscosity lubricants is not so low compared with measured values of 0.003 to 0.02 for natural synovial joints. In natural joints, the viscosity of synovial fluid is reduced to a very low value as twice or several times of water viscosity as non-Newtonian property under a high shear rate of 10^5–10^6 s^{-1} during walking. This discrepancy indicates that simple soft-EHL modelling including elastic soft layer has not sufficiently elucidated the actual lubrication mechanism, although elastic deformation enhances the EHL film thickness.

Dowson and Jin[6] evaluated the possibility of fluid film formation during normal walking by considering the elastic deformation of surface asperity in numerical EHL analysis. In previous studies, minimum EHL film thickness for smooth compliant surface was predicted to be less than 1 μm during walking, and maximum height of the undeformed surface roughness of articular cartilage was estimated to be 1–2 μm or more, and thus, the difficulty in fluid film lubrication was evaluated because of film parameter less than 3 as the ratio of minimum film thickness to composite roughness. In their analysis, however, the flattening of surface asperity in conjunction zone (load-carrying zone) was able to maintain a fluid film thickness of about 0.6 μm without interaction between the rubbing surfaces during walking. This lubricating mechanism was called micro-EHL, which indicates the possibility of fluid film lubrication during normal walking.

On the contrary, at start up after standing for a long time, some local direct contacts appear to occur between the rubbing cartilage surfaces. Under these thin film conditions, mixed lubrication and/or boundary lubrication modes are likely to prevail, and in addition, weeping lubrication[7] and boosted lubrication[8] may become effective. In boundary lubrication regime, the adsorbed films composed of glycoproteins,[9] proteins[10] and/or phospholipids[11] are likely to play roles in friction reduction and protection of surfaces. After removal of adsorbed films on cartilage surfaces, it was pointed out that non-fibrillar proteoglycan gel-like surface layer maintains a low friction due to its low shearing resistance and protects the cartilage bulk tissue.[12] Surface structure covered with adsorbed films on underlying proteoglycan gel-like layer[13] has one kind of fail-safe system in synovial joints. As mentioned above, the various lubrication modes appear to synergistically play important roles in the reduction of friction and wear, depending on the severity of operating conditions. This superior lubrication mechanism was called the adaptive multimode lubrication mechanism by Murakami.[3,14]

In addition to the previously described lubrication modes, the importance of biphasic lubrication[15] and hydration lubrication[16] has been indicated. The molecular lubrication mechanisms including polymer brush[17,18] has been explored.

On the viewpoint of biphasic lubrication,[15,19–21] it should be first recognized that articular cartilage has a high water content from 70% to 80% in tissue composed of type II collagen, proteoglycan and chondrocytes, and thus exhibits a time-dependent biphasic behaviour due to the simultaneous coexistence of solid and liquid phases.[22] It is also noted that lubrication mode depends on the extent of exudation and rehydration. The load support by interstitial fluid pressure in biphasic cartilage controls the friction and deformation. In this article, the difference in effectiveness of load support by interstitial fluid pressure under different loading conditions is examined by biphasic FE analysis previously reported by Sakai et al.[23]

Next, under operating condition where the effectiveness of biphasic lubrication will be reduced, the roles of alternate lubrication mechanisms are

discussed on the basis of reciprocating tests of articular cartilage against glass plate. In intimate local contact zone of hydrated cartilage surface, the effectiveness of rehydration and adsorbed films formed on proteoglycan gel layer at the uppermost superficial zone in articular cartilage was examined in repeated reciprocating tests, including the restarting processes after interruption and unloading to evaluate the influence of rehydration and roles of adsorbed film.[24,25]

Lubrication mechanism in artificial joints

In most of joint prostheses composed of UHMWPE and metal, some direct contacts occur between the rubbing surfaces, which can produce wear debris in mixed or boundary lubrication modes. Although several new trials such as cross-linking of UHMWPE,[26] addition of vitamin E,[27] surface treatment by phospholipid polymeric brush-like layer to UHMWPE[28] and improvement of hard-on-hard bearing[29,30] have extended the life of joint prostheses; there are still unsolved problems on wear under severe contact conditions in various daily activities. Therefore, another promising method to establish no wear and low friction is required. The application of appropriate compliant artificial cartilage materials with properties similar to articular cartilage is expected to duplicate the superior load-carrying capacity and tribological properties of natural synovial joints. The fluid film formation is enhanced and the contact stress level is reduced due to the elastic deformation effect of low-modulus materials in joint prostheses, as described in 'Adaptive multimode lubrication in natural synovial joints'. Unsworth et al.[31] showed in hip prosthesis composed of metallic femoral head and acetabular cup lined with polyurethane of appropriate compliance and thickness that the fluid film lubrication can be achieved even with low-viscosity lubricants in experimental simulator tests. The polyurethane has sufficient mechanical strength, but the possibility of high friction lubricated with lubricant containing synovia constituents under thin film conditions[32] should be prevented. In contrast, poly(vinyl alcohol) (PVA) hydrogel with high water content is expected to reproduce similar multimode lubrication to natural joints.[14,32] At earlier stage (1988), the hip prosthesis with artificial cartilage layer of PVA hydrogel prepared by repeated freezing–thawing method with 85–90 wt% water content on the inner surface of the acetabular cup showed quite a similar low frictional behaviour to natural synovial joint, but did not attain the sufficient durability in the simulator test.[33] Meanwhile, the PVA hydrogel prepared through other synthetic process with lower water content had a better wear resistance in unidirectional pin-on-disc test and exhibited better shock-absorbing ability than traditional UHMWPE. However, wear increased in reciprocating test including thin film condition at stroke ends.[34] The simplified knee prosthesis model with soft layer of PVA hydrogel prepared by repeated freezing–thawing method with high water content of 79 wt% and Young's modulus of 1.1 MPa exhibited superior lower friction in walking simulator test lubricated with hyaluronate (HA) solution containing serum proteins than the model with polyurethane layer as described above.[32] However, an increase in protein concentration in the HA solution increased wear of PVA in reciprocating test of PVA hydrogel against itself under severe conditions.[35] Even in this reciprocating test, at certain combination of albumin and γ-globulin in lubricants, it was found that the wear was remarkably reduced, where the layered adsorbed film formation was confirmed.[35] The fluorescent images of adsorbed films after testing indicated the optimum adsorbed film formation as layered structure at minimum wear and low friction conditions. Furthermore, the corresponding adsorbed film formation during reciprocation was confirmed by in situ visualization.[36–38] But, further improvement of tribological performance of hydrogel artificial cartilage is required for various physiological conditions. The possibility of further improvement by fibre reinforcement in tribological property of PVA hydrogel in artificial joints is examined in this article.

For clinical application, the in vivo study for post-operative 2 years on biocompatibility and stability of meniscal function including mechanical properties of PVA hydrogel artificial meniscus of high water content in rabbit joint[39] suggests a satisfactory possibility of PVA hydrogel meniscal replacement treatment. The authors confirmed the good wear resistance of PVA hydrogel cartilage implanted in femoral chondyle as hemi-arthroplasty in rabbit knee joint as a preliminary evaluation.[40]

Materials and methods

Biphasic FE analysis for articular cartilage during reciprocating motions

In biphasic lubrication, the keeping of high ratio of load support by interstitial fluid pressurization due to very low permeability of cartilage tissue is capable to reduce friction. In the biphasic FE analysis, the changes in interstitial fluid pressure and stress in solid phase in the two models in reciprocating motion were examined. Detailed analysis method is described in the previous paper by Sakai et al.,[23] and the important fundamental method and different terms are described in this article. The biphasic FE analysis was carried out using inhomogeneous depth-dependent apparent Young's modulus of solid phase,[41,42] strain-dependent permeability (compaction effect)[43,44] and collagen reinforcement in tensile strain.[44] In this study, the differences in biphasic behaviours were examined under different loading

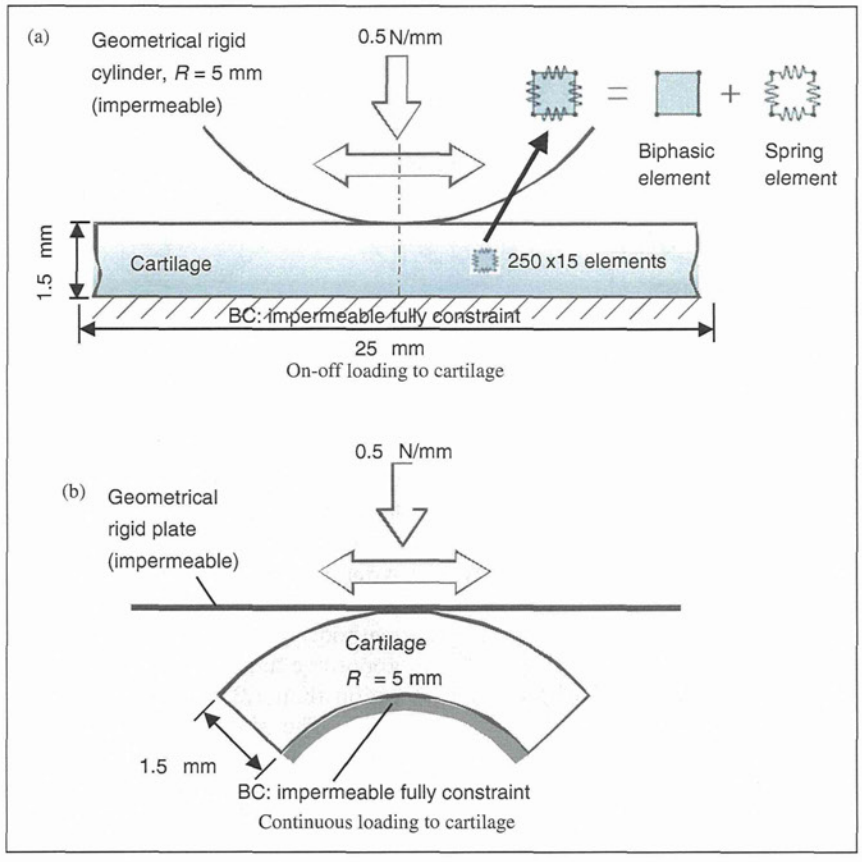

Figure 1. Biphasic FE models for reciprocating sliding under two kinds of loading conditions.

conditions for two models, as shown in Figure 1, in the reciprocating tests at sliding speed 4 mm/s and stroke 8 mm at a constant load of 0.5 N/mm. For model (a) under on–off loading to articular cartilage, the reciprocating sliding of cylindrical impermeable rigid specimen was simulated on the biphasic cartilage flat plate specimen of 1.5 mm thickness where the contact region migrates on the cartilage surface, similar to that described in the previous paper.[23] In contrast, for model (b) under continuous loading to articular cartilage, the reciprocating sliding of impermeable rigid plate specimen was simulated on the biphasic cartilage cylindrical specimen of 1.5 mm thickness where the continuous contact is maintained on the top area of the articular cartilage.

Two-dimensional biphasic FE analysis was conducted using commercial package ABAQUS (6.8-4), which was evaluated as an appropriate software for the biphasic analysis.[45] The biphasic tissue was modelled by CPE4RP (four-node bilinear displacement and pore pressure, reduced integration with hourglass control) elements and the mesh size was chosen as 0.1 mm^2. The horizontal and vertical fibrils were represented by spring element SPRINGA (axial spring between two nodes, whose line of action is the line joining the two nodes) of the software, in which the spring elements were configured to generate reaction force only in the tensile direction. The stiffness K of the spring elements was simplified to the uniform value over the tissue and both in horizontal and vertical directions.

The bottom surfaces of the cartilage models were fixed and impermeable, where no flow was allowed through them. Material properties were specified by curve fitting comparing FE calculation with experimental time-dependent reaction force of the cylindrical indenter. The other surfaces were not fixed and basically permeable except for the contact region. The friction coefficient for solid-to-solid contact μ_{eq} between the geometrical rigid indenter and the solid phase[18] was set to 0.2. In this study, the management of the surface seepage for exuding water content was implemented by user subroutine of ABAQUS using FLOW function (user subroutine to define non-uniform seepage coefficient and associated sink pore pressure for consolidation analysis).

The variables for the curve fitting on FE calculation were as follows:

total apparent Young's modulus: $E_0 = 0.83$ MPa
depth-dependent Young's modulus at depth x

$$E(x) = (\varepsilon_0/\varepsilon)E_0 \quad (1)$$

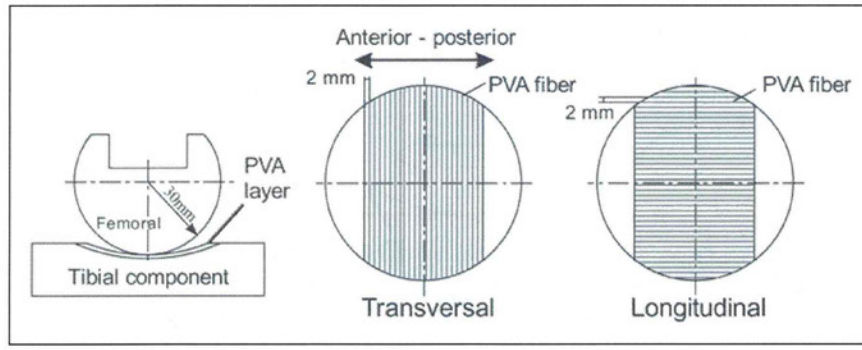

Figure 2. PVA specimens for simulator test.
PVA: poly(vinyl alcohol).

local strain at depth x

$$\varepsilon(x) = 0.462e^{-6.53x} + 0.0284 \quad (2)$$

Poisson's ratio: $\nu = 0.125$
initial permeability: $k_0 = 58.9 \times 10^{-15}\,\mathrm{m}^4/\mathrm{Ns}$
minimum permeability: $k_{\min} = 5.0 \times 10^{-15}\,\mathrm{m}^4/\mathrm{Ns}$
compaction effect of permeability: $M = 22$
initial void ratio: $e_0 = 4.0$ (80% interstitial fluid)
spring stiffness: $K = 17.5\,\mathrm{MPa}$
seepage coefficient: $1\,\mathrm{mm}^3/\mathrm{Ns}$ for flow and $0\,\mathrm{mm}^3/\mathrm{Ns}$ for no flow

The strain dependence of permeability k is estimated by the following formula above the minimum limit, where e is the current void ratio[44]

$$k = k_0 \exp(M(e - e_0)/(1 + e_0)) \quad (3)$$

In simulation of reciprocating test, a load of 0.5 N/mm was applied by rigid cylindrical or flat plate indenter with a ramp time of 1 s and then the load was held constant for further 508 s. Initial horizontal position of the indenter was at the centre of the cartilage tissue surface. The reciprocation of rigid cylinder or flat plate was started immediately after loading and continued for 508 s, 127 cycles at a period of 4 s.

Improvement of tribological performance of artificial cartilage

In the walking simulator test, the simplified knee prosthesis models composed of stainless steel cylindrical femoral component of radius 30 mm and axial length 60 mm, and tibial component with PVA hydrogel layer in 2 mm thickness as a concave surface of radius 60 mm were used (Figure 2).[46] To examine the performance of fibre-reinforced PVA, three kinds of PVA sheets of thickness 2 mm were prepared, i.e. pure PVA and fibre-reinforced PVA in transversal and longitudinal directions to anterior–posterior, as shown in Figure 2. As reinforcing fibre, long-fibre PVA of diameter 0.34 mm and strength 1.9 N was used. PVA fibre was located at the centre in thickness and at definite intervals of 2 mm between the adjacent fibres. After arrangement of fibre network, PVA solution was cast in and gelled by repeated freezing–thawing method. Young's modulus of fibre-reinforced PVA is about five times larger as 5.8 MPa in longitudinal direction than 1.2 MPa in transversal direction or pure PVA. The simulator testing was conducted under normal walking condition for flexion–extension motion and phase-depending tibial-axis load according to the condition in draft of ISO-14243 (1998). The internal–external rotation and anterior–posterior movement were constrained to evaluate the frictional behaviours in sliding motion through load cell. HA solution containing 0.7 wt% albumin and 1.4 wt% γ-globulin was used, because this lubricant showed very low wear and low friction in reciprocating test of sliding pair of PVA against itself.[35,47]

Results

Biphasic FE analysis for articular cartilage during reciprocation motions

The changes in interstitial fluid pressure and Mises stress of solid phase in simulated reciprocating tests based on biphasic FE analysis are shown for the on–off loading to articular cartilage (migrating contact area) and for the continuous loading to articular cartilage (continuous contact) in Figures 3 and 4, respectively. It is noticed under on–off loading condition in Figure 3 that the interstitial fluid pressure is high at start and a high level of pressure is maintained even after 508 s, 127 reciprocating cycles. In addition, Mises stress is low at start and the stress distribution is a little changed but stress level is not so much changed after 508 s, 127 cycles. This fact suggests that most of the loading is supported by interstitial fluid pressure in reciprocating sliding with sufficient stroke length.[48] As pointed out in the previous paper,[23] the model including the spring reinforcement exuded the interstitial fluid in the forward surface of the indenter, whereas the fluid flow in the backward region was

drawn into the cartilage tissue. On the contrary, the continuous loading to the cartilage had a large influence on time-dependent biphasic behaviours. It is remarkably noted under continuous loading to articular cartilage in Figure 4 that the interstitial fluid pressure at start is considerably high and Mises stress at start is low, but after 508 s, 127 reciprocating cycles, the fluid pressure almost disappears and high Mises stress concentrates in the cartilage surface zone. Furthermore, it is worth noting that the contact area increases from the initial contact area, while the contact area under on–off loading maintains almost initial area in size.

To compare the changes in load supports by fluid pressure and vertical stress in solid phase, the supporting forces by fluid pressure and vertical stress in solid phase were estimated and the percentages of fluid load support were calculated in Figure 5. It is confirmed that the fluid load support maintains from 90% at start to 83% after 508 s in reciprocation motion under on–off loading condition, but under a continuous loading condition, the load support by interstitial fluid pressure deceases from 91% at start to 27% after 508 s as time-depending phenomenon. The maintaining of fluid pressure under on–off loading is considered to be due to recovery of deformation with rehydration during off-loading phase, as indicated by a previous paper.[23]

In the biphasic FE analysis for reciprocating sliding, the friction coefficient μ_{eq}[15] for solid-on-solid contact is assumed as 0.2. Therefore, the time-depending changes in friction coefficient μ_{eff} can be estimated using the formula by Ateshian et al.[19,21]

$$\mu_{eff} = \mu_{eq}(1 - (1 - \Psi)W^{\mathcal{P}}/W) \tag{4}$$

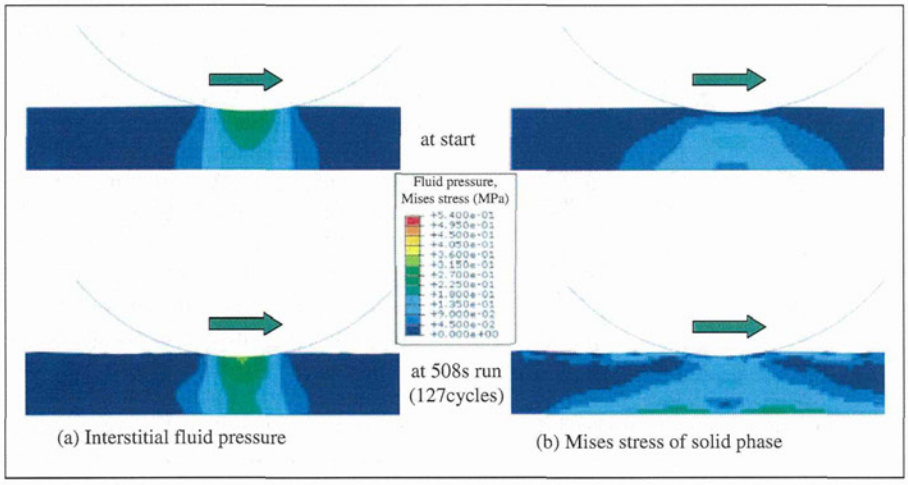

Figure 3. Changes in interstitial fluid pressure and Mises stress of solid phase in the reciprocating test under on–off loading to the cartilage.

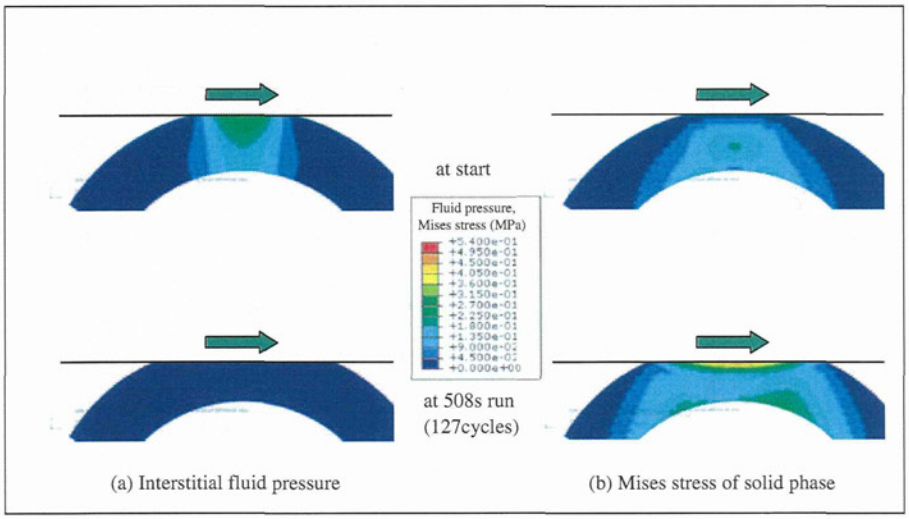

Figure 4. Changes in interstitial fluid pressure and Mises stress of solid phase in the reciprocating test under continuous loading to the cartilage.

where W is the total load support, W^p the load support by fluid pressure and Ψ the fraction of contact area of solid phase.

The estimated frictional behaviours are shown in Figure 6. The friction for on–off loading condition shows a little increase but is not so much changed. In contrast, the friction for continuous loading gradually increases from an initial low value and approaches to equivalent friction coefficient, although the friction level depends on the assumed value of 0.2 for solid-to-solid friction coefficient. The gradual increase in friction under continuous loading corresponds to the previous studies.[15,19,21]

As described above, the biphasic lubrication mechanism is expected to be effective in reciprocating sliding where the contact region of cartilage specimen migrates for the cartilage specimen. However, in reciprocating sliding of cartilage under continuous loading, the interstitial fluid pressurization diminishes with exudation of fluid from the cartilage at a constant load, and thus, the effect of biphasic lubrication is gradually decreased. In the latter case, the alternate lubrication mechanisms become important from the viewpoint of adaptive multimode lubrication, and new findings are discussed on the basis of the previous experimental results of friction tests in 'Discussion'.

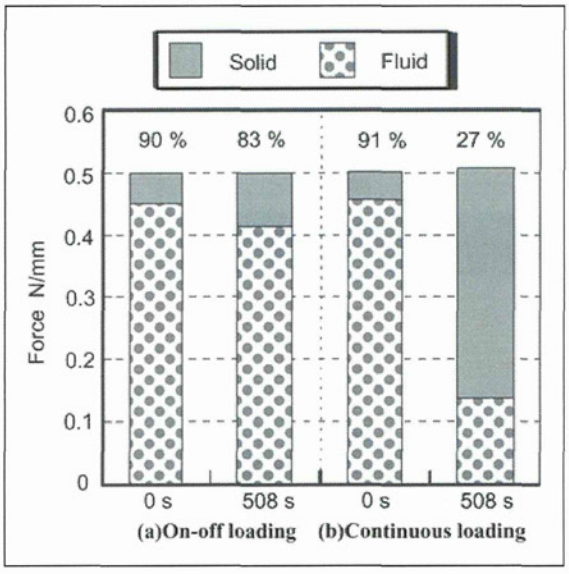

Figure 5. Load support by interstitial fluid pressure and stress in solid phase for on–off loading and continuous loading to cartilage (percentages of load support by fluid pressure are shown with graph).

Improvement of tribological performance of artificial cartilage

Figure 7 shows the frictional behaviours of simplified knee prostheses composed of metallic cylindrical femoral component and tibial component with PVA hydrogel layer in the walking simulator test.[46] HA solution containing 0.7 wt% albumin and 1.4 wt% γ-globulin as one of the optimum composition seems to be effective in maintaining a low friction level during stance phase under high load. For comparison of three models during stance and swing phases, pure PVA shows the largest friction, and fibre-reinforced PVA in the longitudinal direction exhibits the lowest friction (Figure 7). The fibre-reinforced PVA in the transversal direction showed a little higher friction than in longitudinally reinforced PVA. As discussed in the previous paper[23] on biphasic FE analysis, the reinforcement by collagen fibre in the surface zone was effective to maintain the interstitial pressurization during reciprocating sliding. The experimental result in Figure 7 indicates the possibility of application of biphasic lubrication mechanism in natural articular cartilage to hydrogel artificial cartilage. However, the further investigation for actual lubrication mechanism in fibre-reinforced hydrogel is required, including synergistic lubrication with

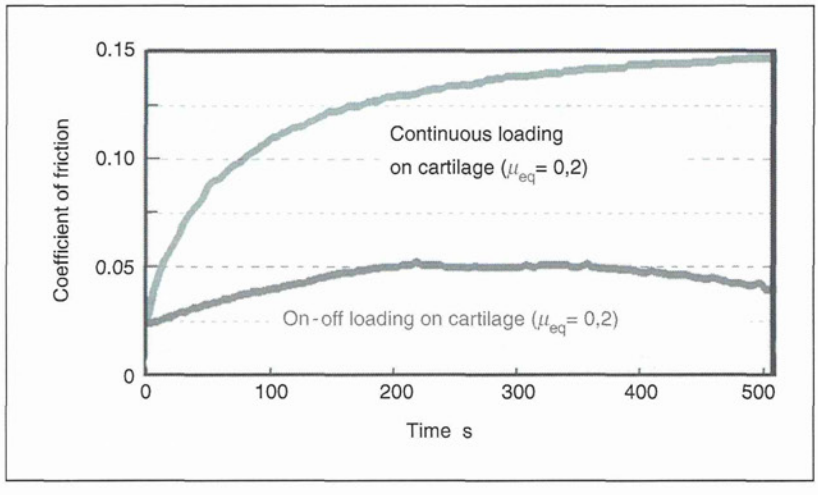

Figure 6. Estimated friction behaviours based on biphasic friction for on–off loading and continuous loading to cartilage in reciprocating motion.